

Figure 2. Plot of cohesive energy versus period number of the periodic table.

the type of orbitals and their principal quantum numbers, the relationship describes the covalent interaction of the valence shells of all neighboring orbitals.

The tabulated van der Waals radii deliver reasonable estimates of the size of atoms for all elements.^[34,35] The recommended crystallographic van der Waals radii^[34] increase within each group and for many elements the suggested values are larger than those of subsequently published van der Waals radii, which are characterized as consistent for all main-group elements.^[35] The larger atom size of B than that of Al in this work is not supported by the cohesive energies. The dependences in Figure 2 reflect the strong increase of the van der Waals diameter between periods two and three, compared with a smaller change between the higher periods. This enlargement of atom size induces an alteration of hybridization from planar sp^2 to buckled sp^2 - sp^3 hybrids from graphene to its higher homologues (see Figure 3). Owing to the reduced orbital overlap, mixed sp^2 - sp^3 hybrids become more stable for silicene



Prof. Dr. Peter Hess is professor (emeritus) of Physical Chemistry at the University of Heidelberg since 1980. He has been active in laser-based photoacoustic trace gas analysis, surface acoustic waves (SAWs), and wedge and solitary surface waves employed to study all-optical nondestructive evaluation (NDE), elastic properties, and fracture strength of solids. Other fields were silicon surface spectroscopy and chemistry. As emeritus he became interested in bonding, structure, and mechanical behavior of 2D materials. He produced more than 300 publications and was editor or co-editor of six books. He received the James Smith prize of IPPA and served as director of the Technology Transfer Center Heidelberg for laser processing.

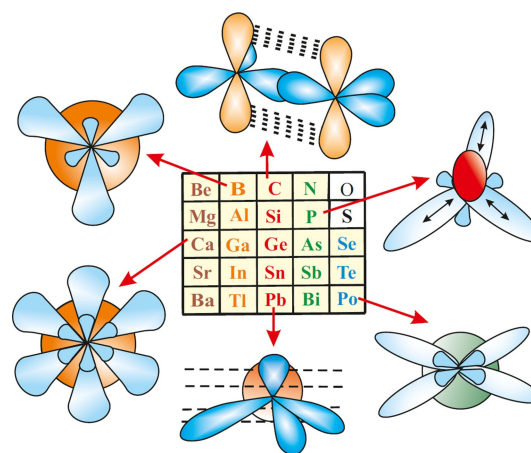


Figure 3. Schematic presentation of hybrids of main group elements of the periodic table.

and with increasing sp^3 contribution corrugation increases and binding energy decreases for the higher homologues.

Note that measurements of the thickness of planar monolayers by atomic force microscopy (AFM) are in good agreement with tabulated van der Waals diameters.^[36] The exceptionally small atom radius given for Be^[35] implies much stronger bonding of Be than the larger crystallographic value, consistent with calculated cohesive energies. The almost constant cohesive energies of the higher homologues of Be, despite strong increase of atom size, point to weaker metallic bonding.

A plot of bond lengths of group II–VI monolayers versus period number shows the expected significant elongation of bonds between periods two and three, followed by an asymptotic behavior, qualitatively reflecting the increase of the van der Waals diameters (see Figure 4). Different from the mean cohesive energy the individual bond energies and bond lengths may vary in corrugated structures. In the case of different bond lengths, the plot displays the shortest one. In total, the bond length increases by a factor of about three from graphene with

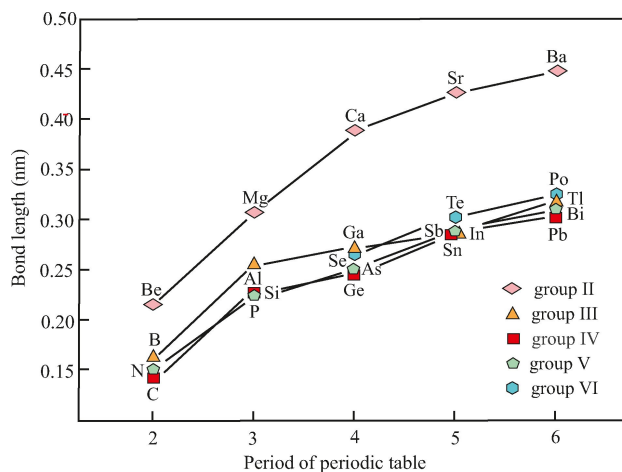


Figure 4. Plot of the bond length versus period number of the periodic table.

Table 1. A selection of cohesive energies and bond lengths of group-II–VI monolayers (ML).

ML	Structure, space group	Cohesive energy [eV atom ⁻¹]	Bond length, d ₁ , d ₂ (lattice const.) [nm]
beryllene	hexagonal six neighbors	−2.91 ^[5]	0.215 ^[5]
	planar honeycomb	−3.00 ^[6]	(0.213) ^[6]
magnesium	hexagonal six neighbors	−0.91 ^[5]	0.307 ^[5]
	planar honeycomb	−0.95 ^[6]	(0.306) ^[6]
calcene	hexagonal six neighbors	−1.09 ^[5]	0.388 ^[5]
	planar honeycomb	−1.18 ^[6]	(0.387) ^[6]
strontene	hexagonal six neighbors	−0.85 ^[5]	0.427 ^[5]
	planar honeycomb	−0.97 ^[6]	(0.425) ^[6]
barium	hexagonal six neighbors	−1.04 ^[5]	0.448 ^[5]
	planar honeycomb	−1.20 ^[6]	(0.447) ^[6]
borophene	planar β _{12r} , <i>Pmm2</i> ^[7]	−6.15 ^[7] , −5.71 ^[8]	0.165–0.170 ^[9]
	planar γ _{3r} , <i>Cmmm</i> ^[7]	−6.16 ^[7] , −5.72 ^[8]	0.160–0.171 ^[9]
aluminum	planar, <i>P6/mmm</i> ^[10]	−1.96 ^[10] , −2.32 ^[11]	0.259 ^[10] , 0.257 ^[11]
	buckled, <i>P-3m1</i>	−3.27 ^[11]	0.265, 0.275 ^[12]
gallene	planar, a ₁₀₀ -Ga, <i>Pbam</i> ^[13]		0.266, 0.267 ^[13]
	puckered, b ₀₁₀ -Ga	−2.32 ^[14]	0.271, 0.273 ^[14]
indium	planar, <i>P6/mmm</i> ^[16]	−1.81 ^[15] , −2.08 ^[16]	0.286 ^[15] , 0.282 ^[16]
	buckled, <i>P3m1</i> ^[16]	−1.83 ^[15] , −2.13 ^[16]	0.289 ^[15] , 0.302 ^[16]
thallium	hexagonal six neighbors	−1.67 ^[5]	0.331 ^[5]
	planar honeycomb	−1.65 ^[6]	(0.332) ^[6]
graphene	planar, <i>P6/mmm</i> ^[20]	−7.85 ^[17] , −7.82 ^[18]	0.142 ^[17] , 0.142 ^[18,19]
silicene	low buckled, <i>P-3m1</i> ^[20]	−3.91 ^[17] , −3.86 ^[18]	0.228 ^[17] , 0.227 ^[18,19]
germanene	low buckled, <i>P-3m1</i> ^[20]	−3.24 ^[17] , −3.19 ^[18]	0.244 ^[17] , 0.242 ^[18,19]
stanene	high buckled, <i>P-3m1</i> ^[20]	−2.73 ^[17] , −2.65 ^[18]	0.284 ^[17] , 0.283 ^[18,19]
plumbene	high buckled, <i>P-3m1</i> ^[20]	−2.28 ^[18]	0.302 ^[21] , 0.300 ^[18]
nitrogen	buckled, hb, <i>P-3m1</i>	−6.81 ^[22] , −3.67 ^[23]	0.149 ^[23] , 0.150 ^[23,24]
	puckered, sw, <i>Pmna</i> ^[27]	−3.59 ^[25] , −3.16 ^[27]	0.222, 0.226 ^[26]
phosphorene	buckled, hb, <i>P-3m1</i> ^[27]	−3.55 ^[25] , −3.14 ^[27]	0.226 ^[26] , 0.226 ^[23]
	puckered, sw, <i>Pmna</i> ^[27]	−3.13 ^[25] , −2.85 ^[27]	0.250, 0.248 ^[26]
arsenene	buckled, hb, <i>P-3m1</i> ^[27]	−3.14 ^[25] , −2.89 ^[27]	0.251 ^[26] , 0.245 ^[23]
	puckered, aw, <i>Pmn2</i> ₁ ^[27]	−1.77 ^[26] , −2.56 ^[27]	0.290, 0.284 ^[26]
antimonene	buckled, hb, <i>P-3m1</i> ^[27]	−1.96 ^[26] , −2.57 ^[27]	0.287 ^[26] , 0.287 ^[23]
	puckered, aw, <i>Pmn2</i> ₁ ^[27]	−1.38 ^[26] , −2.42 ^[27]	0.306, 0.298 ^[26]
bismuthene	buckled, hb, <i>P-3m1</i> ^[27]	−1.44 ^[26] , −2.41 ^[27]	0.301 ^[26] , 0.307 ^[23]
selenene	tetragonal	−2.71 ^[28] , −2.77 ^[29]	0.265–0.338 ^[29]
	rhombic, <i>P-3m1</i>	−2.56 ^[28] , −2.72 ^[29]	0.266 ^[29]
tellurene	monoclinic, <i>Cm</i> ^[30]	−2.65 ^[30]	0.240, 0.271 ^[30]
	tetrag., <i>P2/m</i> , <i>P2₁/m</i> ^[32]	−2.56 ^[31]	0.275, 0.302 ^[31]
polonium	rhombic, <i>P-3m1</i> ^[32]	−2.62 ^[31]	0.302 ^[31]
	monoclinic, <i>Cm</i> ^[30]	−2.51 ^[30]	0.287, 0.305 ^[30]
poloniumene	square lattice structure	−2.58 ^[33]	0.318 ^[33]
	hexagonal six neighbors	−2.35 ^[33]	0.334 ^[33]
	honeycomb structure	−2.33 ^[33]	0.312 ^[33]

the shortest bond of 0.142 nm,^[17] to Ba with the longest bond of 0.448 nm,^[5] while the corresponding cohesive energy changes by a factor of about eight from −7.85 eV/atom,^[17] to −1.04 eV/atom,^[5] respectively. Within the errors involved in such first-principles calculations this enormous decrease of the cohesive energy supports the theoretically predicted inverse quadratic dependence predicted by tight-binding theory.^[26]

Figure 5 shows the calculated cohesive energies of main-group elements versus column number. The plot reveals again the pronounced change of binding energies between the second and third period. From the second to the fifth period, in the dependences of the individual periods, the group-IV monolayers exhibit the maximum bonding strength. This demonstrates that the four valence electrons form the most stable 2D bonds with their noble gas configuration ('octet rule').

Along each period the effect of the varying number of valence electrons dominates bonding over minor contributions from the varying atom size. The regular pattern of cohesive 2D interaction observed for the five periods is a consequence of the 'aufbau' principle of electron shells in the periodic table.

The deficiency of valence electrons in group II–III compounds causes a drastic decrease of cohesive energy (see Figure 5). Boron, for example, with its three valence electrons can form 2D networks, however, the available bonding orbitals are partially empty. According to tight-binding theory, based on the linear combination of atomic orbitals (LCAO) and the hybridization concept, not all three valence electrons are in bonding orbitals and therefore, the uniform trivalent network is not stable.^[37] Note that the experimentally synthesized planar monolayers of boron, included in Table 1, contain a mixture of

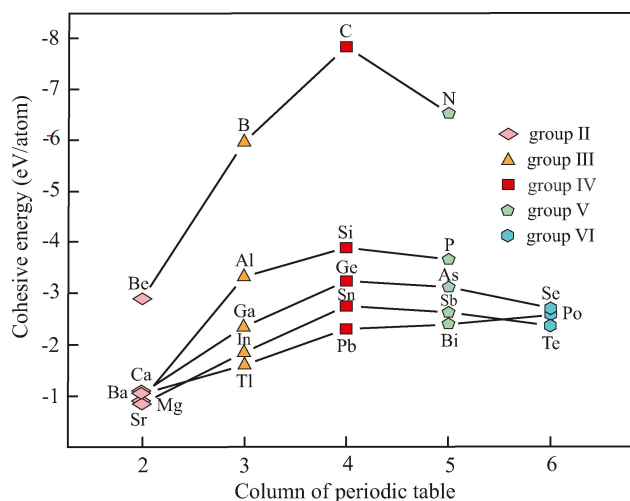


Figure 5. Plot of cohesive energy versus column number of the periodic table.

triangular and hexagonal motifs. A change in the type of bonding to weaker metallic interaction leads to an even larger reduction of the cohesive energies in group-II monolayers. Metallic bonding usually prefers a large coordination with six nearest neighbors (see Figure 3), which in group-II monolayers has a comparable low binding energy as the planar honeycomb configuration (see Table 1).

A surplus of valence electrons in groups V–VI has a much smaller effect on the binding energy. In pnictogens, with five valence electrons, tetrahedral-like hybrids with a backbone consisting of three σ bonds and a lone-electron pair lead to dynamically stable puckered and buckled structures with an equilibrium configuration controlled by the repulsion of the lone-electron pairs (see Figure 3). Interestingly, the binding energies of the two allotropes often are comparable and may lead to the synthesis of their mixtures (see Table 1). While a three-dimensional solid of N does not seem to be stable, 2D buckled nitrogene is thermodynamically and dynamically stable.^[22–24] Owing to the multivalency of chalcogenides with oxidation states -2 and $+6$, the group-VI elements exist in diverse hybrids and form low-symmetry structures that no longer exhibit hexagonal symmetry such as trigonal, tetragonal, rhombic, monoclinic, and square phases. The transition to metallic-type bonding in this column from Se to Po seems to be the main reason for comparable bonding strengths and small deviations from the regular dependence of the heavy compounds (see Figure 5). As an example, Figure 3 shows the rare square lattice with tetra-coordination of metallic poloniumene, specified in Table 1.

Figure 6 displays the variation of bond length (for group II also lattice constants) with the column number. The minima of the group-IV bond lengths are consistent with the maxima of the cohesive energies in Figure 5. On the side of deficiency of valence electrons with respect to group-IV monolayers, a strong increase of bond length and enormous weakening of bonding occurs, whereas the bond length increases only slightly on the

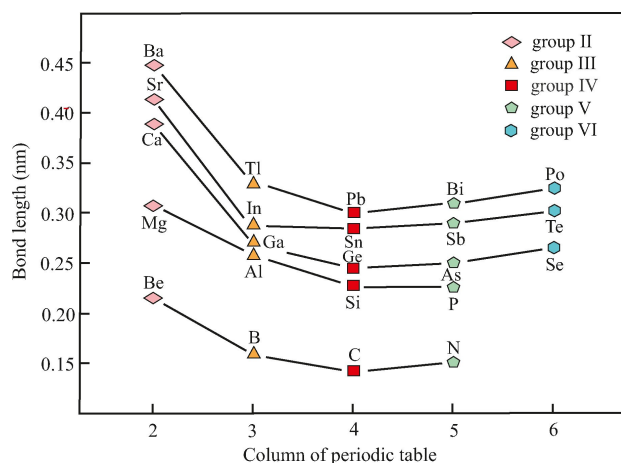


Figure 6. Plot of the bond length versus column number of the periodic table.

side with a surplus of valence electrons and agrees for silicene and phosphorene. The diagrams reveal different consequences of electron deficiency and a surplus of valence electrons on bonding. The deficiency of valence electrons leads to only partially filled bonding orbitals with an essential loss of bonding power, e.g., in the delocalized three-centered bonds of boron. One of the three electrons even occupies an in-plane antibonding orbital.^[37] Conversely, when the valence shells contain additional electrons, it is possible to fill the bonding orbitals completely. However, the surplus of electrons may reduce the binding energy and extend bond lengths slightly, e.g., by the repulsion effect of lone-electron pairs.

In summary, both, σ and π bonds react flexible on the restriction to 2D space, the variation of atom size, and deviations of the number of valence electrons from the octet rule. The diversity of corrugated atomic monolayers demonstrates variable covalent and metallic-like bonding with novel types of hybridization and coordination, surpassing by far the number of perfect planar structures. Detailed understanding of the bonding behavior of elemental monolayers allows a useful prediction of bonding in the large family of their binary, e.g., SiC, and isoelectronic compounds, e.g., h-BN, by taking the mean values of binding energies and bond lengths of the two constituents.⁴

The diagrams of the cohesive energy and bond length versus period number and column number reveal the two main factors controlling type and strength of 2D bonding and structure of main-group II–VI monolayers. Covalent 2D bonding depends on the inherent periodicity of atom size of the columns, mostly following the tabulated van der Waals diameter. Furthermore, the periodic variation of the number of valence electrons along the periods describes the performance of the groups with a deficiency or a surplus of valence electrons in comparison with octet stability. The atomic orbital-hybridization concept offers a simple explanation of these fundamental findings. The 2D bonding-structure relation is consistent with an inverse quadratic relationship between covalent

bonding and bond length. Weaker metallic-type interaction appears for group-II and group-VI monolayers, as well as period-VI monolayers, with large separation from the graphene position in the periodic table. This position may be identified as the center of perfect covalent bonding. Hence, the predictive power of the periodic table gives access to general guidelines of 2D bonding and structure formation and allows an assessment of published data.

Notes

The opinions expressed in this publication are the view of the author(s) and do not necessarily reflect the opinions or views of *ChemPhysChem*, the Publisher, or the affiliated editors.

Acknowledgements

Open Access funding enabled and organized by Projekt DEAL.

Conflict of Interest

There are no conflicts of interest to declare.

Keywords: nanoscience · monolayers · 2D bonding · bond length · periodic table

- [1] J. Gao, Z. Xu, S. Chen, M. S. Bharathi, Y.-W. Zhang, *Adv. Theory Simul.* **2018**, *1*, 1800085.
- [2] B. Liu, K. Zhou, *Prog. Mater. Sci.* **2019**, *100*, 99–169.
- [3] A. J. Mannix, B. Kiraly, M. C. Hersam, N. P. Guisinger, *Nat. Chem. Rev.* **2017**, *1*, 0014.
- [4] P. Hess, *Nanoscale Horiz.* **2021**, *6*, 856–892.
- [5] J. Navalaita, P. Koskinen, *Phys. Rev. B* **2018**, *97*, 035411.
- [6] S. Ono, *Phys. Rev. B* **2020**, *102*, 165424.
- [7] B. Peng, H. Zhang, H. Shao, Z. Ning, Y. Xu, G. Ni, H. Lu, D. W. Zhang, H. Zhu, *Mater. Res. Lett.* **2017**, *5*, 399–407.
- [8] X. Wu, J. Dai, Y. Zhao, Z. Zhuo, J. Yang, X. C. Zeng, *ACS Nano* **2012**, *6*, 7443–7453.
- [9] B. Mortazavi, O. Rahaman, A. Dianat, T. Rabczuk, *Phys. Chem. Chem. Phys.* **2016**, *18*, 27405–27413.
- [10] C. Kamal, A. Chakrabarti, M. Ezawa, *New J. Phys.* **2015**, *17*, 083014.
- [11] I. Lukačević, M. V. Pajtler, M. Mužević, S. K. Gupta, *J. Mater. Chem. C* **2019**, *7*, 2666–2675.
- [12] B. A. Khalil, N. Gaston, *J. Phys. Condens. Matter* **2021**, *33*, 125901.
- [13] M. Nakhuae, M. Yagmurcukardes, S. A. Ketabi, F. M. Peeters, *Phys. Chem. Chem. Phys.* **2019**, *21*, 15798–15804.
- [14] S. V. Badalov, M. Yagmurcukardes, F. M. Peeters, H. Sahin, *J. Phys. Chem. C* **2018**, *122*, 28302–28309.
- [15] D. Singh, S. K. Gupta, I. Lukačević, Y. Sonvane, *RSC Adv.* **2016**, *6*, 8006–8014.
- [16] D. Singh, S. K. Gupta, I. Lukačević, M. Mužević, Y. Sonvane, R. Ahuja, *Sci. Rep.* **2019**, *9*, 17300.
- [17] J. C. Garcia, D. B. de Lima, L. V. C. Assali, J. F. Justo, *J. Phys. Chem. C* **2011**, *115*, 13242–13246.
- [18] A. Mahmood, G. Rahman, *J. Phys. Condens. Matter* **2020**, *32*, 205501.
- [19] R. John, B. Merlin, *Cryst. Struct. Theory Appl.* **2016**, *5*, 43–55.
- [20] S. M. Farzaneh, S. Rakheja, *Phys. Rev. B* **2021**, *104*, 115205.
- [21] S. Mahmud, Md. K. Alam, *RSC Adv.* **2019**, *9*, 42194–422030.
- [22] Y. Zhang, J. Lee, W.-L. Wang, D.-X. Yao, *Comput. Mater. Sci.* **2015**, *110*, 109–114.
- [23] F. Ersan, D. Kecik, V. O. Özçelik, Y. Kadioglu, O. Ü. Aktürk, E. Durgun, E. Aktürk, S. Ciraci, *Appl. Phys. Rev.* **2019**, *6*, 021308.
- [24] J. Lee, W.-C. Tian, W.-L. Wang, D.-X. Yao, *Sci. Rep.* **2015**, *5*, 11512.
- [25] F. Ersan, E. Aktürk, S. Ciraci, *Phys. Rev. B* **2017**, *96*, 205434.
- [26] S. Guo, W. Zhou, B. Cai, K. Zhang, S. Zhang, H. Zeng, *Nanoscale Horiz.* **2019**, *4*, 1145–1152.
- [27] N. A. P. Namari, M. Saito, *Jpn. J. Appl. Phys.* **2019**, *58*, 061003.
- [28] D. Wang, L.-M. Tang, X.-X. Jiang, J.-Y. Tan, M.-D. He, X.-J. Wang, K.-Q. Chen, *Adv. Electron. Mater.* **2019**, *5*, 1800475.
- [29] L. Ramírez-Montes, W. López-Pérez, R. González-Hernández, C. Pinilla, *Int. J. Quantum Chem.* **2020**, e26267.
- [30] L. Xian, A. P. Paz, E. Bianco, P. M. Ajayan, A. Rubio, *2D Mater.* **2017**, *4*, 041003.
- [31] Z. Zhu, X. Cai, S. Yi, J. Chen, Y. Dai, C. Niu, Z. Guo, M. Xie, F. Liu, J.-H. Cho, Y. Jia, Z. Zhang, *Phys. Rev. Lett.* **2017**, *119*, 106101.
- [32] Y. Xiang, S. Gao, R.-G. Xu, W. Wu, Y. Leng, *Nano Energy* **2019**, *58*, 202–210.
- [33] S. Ono, *Sci. Rep.* **2020**, *10*, 11810.
- [34] S. S. Batsanov, *Inorg. Mater.* **2001**, *37*, 871–885.
- [35] M. Mantina, A. C. Chamberlin, R. Valero, C. J. Cramer, D. G. Truhlar, *J. Phys. Chem. A* **2009**, *113*, 5806–5812.
- [36] P. Hess, *Nanoscale Horiz.* **2020**, *5*, 385–399.
- [37] H. Tang, S. Ismail-Beigi, *Phys. Rev. Lett.* **2007**, *99*, 115501.

Manuscript received: December 13, 2021
Version of record online: February 24, 2022